Macromolecules

Article

pubs.acs.org/Macromolecules

# Transient and Average Unsteady Dynamics of Single Polymers in Large-Amplitude Oscillatory Extension

Yuecheng Zhou[†] and Charles M. Schroeder*[,†,‡,§]

[†]Department of Materials Science and Engineering, [‡]Department of Chemical and Biomolecular Engineering, and [§]Center for Biophysics and Quantitative Biology, University of Illinois at Urbana−Champaign, Urbana, Illinois 61801, United States

**ABSTRACT:** Oscillatory rheometry has been widely used in bulk rheological measurements of complex fluids such as polymer solutions and melts. Despite recent progress on bulk oscillatory rheology, however, the vast majority of single polymer studies has focused on chain dynamics in simple on/off step strain-rate experiments. In order to fully understand dynamic polymer microstructure and to establish connections with bulk rheology, there is a clear need to study the dynamics of single polymers in more realistic, nonidealized model flows with transient forcing functions. In this work, we study the dynamics of single polymers in large amplitude oscillatory extensional (LAOE) flow using experiments and Brownian dynamics (BD) simulations, and we characterize transient polymer stretch, orientation angle, and average unsteady stretch as functions of the flow strength (Weissenberg number, *Wi*) and probing frequency (Deborah number, *De*). Small and large amplitude sinusoidal oscillatory extensional flow are generated in a cross-slot microfluidic geometry, which is facilitated by using an automated flow device called the Stokes trap. This approach allows the conformational dynamics of single DNA molecules to be observed in oscillatory extensional flow for long times. In this way, we observe a characteristic periodic motion of polymers in LAOE including compression, rotation, and stretching between the time-dependent principal axes of extension and compression. Interestingly, distinct polymer conformations are observed in LAOE that appear to be analogous to buckling instabilities for rigid or semiflexible filaments under compression. Average unsteady polymer extension is further characterized for single polymers in oscillatory extension across a wide range of *Wi* and *De*. In the limit of low *Wi*, average polymer stretch is interpreted using analytical results based on a Hookean dumbbell model, which can be used to define a critical *Wi* at the linear to nonlinear transition in oscillatory extension. These results reveal the existence of a master curve for average polymer stretch when plotted as a function of an effective Weissenberg number $Wi_{eff}$. Experimental results are compared to BD simulations, and we observe good agreement between simulations and experiments for transient and average unsteady dynamics. Finally, average transient dynamics in oscillatory extensional flow are further interpreted in the context of Pipkin space, defined by the two-dimensional space described by *Wi* and *De*.

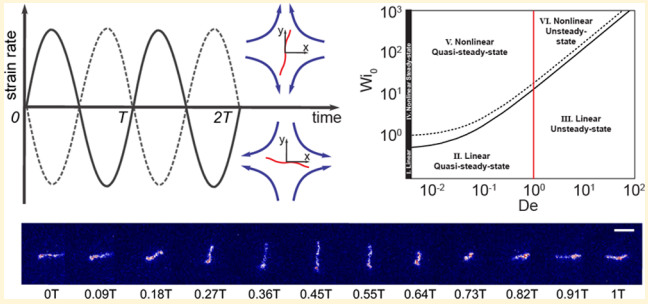


## INTRODUCTION

Dynamic oscillatory rheometry has been widely used to investigate the rheological behavior of complex fluids such as polymer solutions,[1] polymer blends,[2] entangled polymer melts,[3] block copolymers,[4] and colloidal suspensions.[5] Oscillatory shear is one of the most common bulk rheology measurements used to interrogate soft materials and complex fluids. In particular, small amplitude oscillatory shear (SAOS) is a classic method to probe the linear viscoelastic properties of materials based on established physical principles in the limit of small deformation.[6,7] Using this approach, materials are interrogated under small magnitude sinusoidal strains, and the time-dependent stress response is measured. Linear viscoelastic measurements can be used to determine material functions such as the elastic modulus $G'(\omega)$ and the loss modulus $G''(\omega)$, where both linear viscoelastic moduli are independent of the applied strain, provided that the strain amplitude is small. Although SAOS is a convenient and useful method to probe rheological behavior, it is mainly used to study only the linear response properties of materials. In most practical applications involved in processing, however, materials are exposed to highly nonlinear and nonequilibrium flow conditions, thereby inducing polymer deformation under large strains and strain rates during extrusion or related processes.[8] Moreover, vastly different complex fluids may yield deceivingly similar linear viscoelastic signatures because small magnitude strains are insufficient to distinguish fine-scale structural differences at the nano- to microscale.[9,10] Indeed, for many complex materials, the distinguishing rheological signatures may be buried in the nonlinear stress response, despite showing apparently similar linear viscoelastic responses. From this perspective, there is a strong need to characterize the nonlinear rheological properties of complex materials.

In recent years, large amplitude oscillatory shear (LAOS) has been widely employed to investigate the nonlinear rheological properites of materials. LAOS can be implemented using fairly

**Received:** July 26, 2016
**Revised:** September 16, 2016
**Published:** October 5, 2016





DOI: 10.1021/acs.macromol.6b01606
*Macromolecules* 2016, 49, 8018−8030

standard experimental tools including a sliding plate rheometer (SPR)[11] or Fourier transform (FT) rheology based on a commercial rheometer.[12] LAOS is generally performed over a wide range of strain amplitude and frequency,[13] thereby revealing the nonlinear rheological response of materials. In addition, LAOS is performed as a smooth and continuous process without sudden or discontinuous jumps in applied strain or strain rate,[11] which differs from several other nonlinear transient rheological measurements such as step strain experiments. In this way, LAOS can be implemented to effectively achieve robust control over the strain input with reduced experimental noise. However, the challenge lies in interpreting the stress response obtained from LAOS experiments because the transient stress cannot generally be described using linear viscoelastic theories due to the presence of higher order harmonics or strong nonlinearities. To address this issue, Wilhelm et al.[14] employed the Fourier transform (FT) method to analyze the shear stress response as spectra in Fourier space. Ewoldt et al.[15] used a set of first kind orthogonal Chebyshev polynomials to characterize the nonlinear stress response, and this method was based on a nonlinear stress decomposition (SD) method.[16] In this way, certain complex fluids can be uniquely "fingerprinted".[17] Rogers et al.[18] described the nonlinear stress response as purely elastic to purely viscous sequences of processes to extract fundamental physical interpretations of dynamics. In addition to experimental work, Radhakrishnan and Underhill[19] studied the LAOS response of a dilute polymer−nanoparticle mixture with short-ranged attractive interactions using Brownian dynamics (BD) simulations. A frequency sweep was performed with a fixed peak strain rate above the critical polymer globule−stretch transition strain rate, and transitions between different conformational states were identified.

In addition to shear rheology, extensional rheology has also been used to study the nonlinear properties of complex fluids. Extensional flow is considered a strong flow that is very efficient at unraveling flexible macromolecules or aligning semiflexible biofilaments.[20] In recent years, large amplitude oscillatory extension (LAOE) has been developed for bulk-level studies of materials. Using this approach, Rasmussen et al.[21] and Bejenariu et al.[22] examined the soft elasticity of polystyrene (PS) melts and cross-linked polydimethylsiloxane (PDMS) networks using a customized filament stretching rheometer (FSR).[20,23] A unique periodic response for the elongational stress $\tau_{xx} - \tau_{rr}$ was measured in LAOE that is analogous to the periodic response of shear stress $\tau_{xy}$ in LAOS. However, the application of bulk extensional rheometry can be quite challenging for some materials due to gravitational effects for high viscosity samples, which could limit the range of strain rates that can be explored.[20] These problems can be mitigated by using microfluidic cross-slot devices to generate high strain rate planar extensional flow. Odell and Carrington[24] first developed the extensional flow oscillatory rheometer (EFOR) using a cross-slot microfluidic geometry and four electronically driven piezoelectric pumps. Here, flow-induced conformational changes to macromolecules are detected using optical birefringence. Using this approach, Haward and co-workers[25,26] measured the extensional viscosity of dilute polymer solutions from the transient birefringence response in flow. Recently, the geometry of the microfluidic cross-slot device for EFOR was optimized to achieve precise extensional flow profiles across the entire cross-slot region for a wide range of strain rates.[27]

Bulk rheological techniques are essential in measuring macroscopic stress in complex materials. Nevertheless, these methods can only be used to indirectly infer flow-induced deformation at the molecular scale. Single molecule techniques, on the other hand, allow for the direct observation of dynamic microstructure in nonequilibrium flow. Recent advances in single molecule fluorescence imaging have enabled the direct observation of single polymer dynamics in simple model flows such as shear flow,[28−33] planar extensional flow,[34−36] and linear mixed flows.[37,38] However, the vast majority of single polymer studies has only focused on chain dynamics using an idealized on/off flow rate conditions or simple step forcing functions. In many processing applications, polymers experience complex time-dependent flows such as oscillatory extension for flow through porous media or in wavy-wall channels.[39] For these reasons, there is a general need to understand the role of transient oscillatory flows on the dynamics of polymers and to establish a connection between single polymer dynamics and bulk oscillatory rheometry. In this work, we use a single polymer approach to directly probe the dynamics of DNA molecules in oscillatory extension using precisely controlled flows.

Recently, Zhou and Schroeder reported the use of single polymer LAOE to construct molecular stretch−strain rate curves, which are defined as single molecule Lissajou curves.[40] The shapes of the single molecule Lissajou curves were interpreted in the context of polymer chain conformation over a wide range of flow strength (Weissenberg number, $Wi$) and probing frequency (Deborah number, $De$).[40] In the present article, we extend beyond this prior work by characterizing the transient stretch and transient orientation angle for single polymers in LAOE, and these quantities are analyzed using autocorrelation and cross-correlation functions to probe the underlying physics. In addition, we further study average polymer extension in LAOE, and our results reveal a critical flow strength $Wi_{0,crit}$ at which a linear to nonlinear transition in stretching behavior is observed. Moreover, we interpret average stretch results using an analytical model based on a Hookean dumbbell in time-dependent oscillatory extensional flow. Finally, transient polymer conformations are characterized in the context of the two-dimensional space defined by $Wi$ and $De$, which is generally known as Pipkin space. Taken together, these results provide new insights into the dynamics of single polymer chains in controlled time-dependent flows.

## EXPERIMENTAL METHODS

**Materials.** In this work, we study the dynamics of double-stranded $\lambda$-phage DNA (48.5 kbp, New England Biolabs) in oscillatory extension. $\lambda$-DNA is fluorescently labeled with an intercalating dye (YOYO-1, Thermo Fisher, Molecular Probes) with a dye-to-base pair ratio of 1:4 for >1 h in the dark at room temperature. DNA is labeled in an aqueous buffer containing 30 mM Tris/Tris-HCl (pH 8.0), 2 mM EDTA, and 5 mM NaCl. Fluorescently labeled $\lambda$-DNA is then added to an imaging buffer containing 30 mM Tris/Tris-HCl (pH 8.0), 2 mM EDTA, 5 mM NaCl, sucrose (60% w/w), glucose (5 mg/mL), glucose oxidase (0.05 mg/mL), catalase (0.01 mg/mL), and 4% v/v $\beta$-mercaptoethanol. Sucrose is used to increase the solvent viscosity of the imaging buffer solution to 48.5 ± 1 cP at 22.5 °C, which was measured using a cone and plate viscometer (Brookfield). Glucose oxidase/catalase is used as a coupled enzymatic oxygen scavenging system to suppress photobleaching and photocleaving of fluorescently labeled DNA. The concentration of labeled DNA in the imaging buffer is $\sim 10^{-5} c^*$, where $c^*$ is the polymer overlap concentration, thereby yielding an ultradilute solution in the absence



DOI: 10.1021/acs.macromol.6b01606
Macromolecules 2016, 49, 8018−8030

of polymer−polymer interactions. The contour length of fluorescently labeled $\lambda$-DNA is taken to be 21.5 $\mu$m under these conditions.[41]

**Optics and Imaging.** Imaging is performed using an inverted epifluorescence microscope (IX71, Olympus) coupled to an electron-multiplying charge coupled device (EMCCD) camera (iXon, Andor Technology). Labeled DNA samples are illuminated using a 100 W mercury arc lamp (USH102D, UShio) directed through a 3% neutral density filter (Olympus), a 482 ± 18 nm band-pass excitation filter (FF01-482/18-25, Semrock), and a 488 nm single-edge dichroic mirror (Di01-R488-25×36, Semrock). Fluorescence emission is collected by a 1.45 NA, 100× oil immersion objective lens (UPlanSApo, Olympus), and a 488 nm long pass filter (BLP01-488R-25, Semrock) is used in the detection path. Finally, images are acquired by an Andor iXon EMCCD camera (512 × 512 pixels, 16 $\mu$m pixel size) under frame transfer mode at a frame rate of 30 Hz.

**Microfluidic Devices.** Standard techniques in soft lithography are used to fabricate single layer microfluidic devices from polydimethylsiloxane (PDMS) with a base-to-cross-linker ratio of 5:1.[42,43] PDMS devices are bonded to a glass coverslip following oxygen plasma cleaning. The PDMS/glass hybrid microfluidic device is composed of two orthogonal microfluidic channels to form a cross-slot geometry. The inlet/outlet channels are 10 mm long, 400 $\mu$m wide, and 90 $\mu$m in depth, and each channel terminates at an inlet port with a diameter of 1.6 mm. DNA imaging is performed in the region near the center of the cross-slot (imaging area approximately 80 $\mu$m × 80 $\mu$m in size). Pressure-driven flow is used to generate a planar extensional flow in the cross-slot geometry, as described below.

**Particle Tracking Velocimetry.** The flow field is characterized prior to single polymer experiments using particle tracking velocimetry (PTV). Using this approach, fluorescent polystyrene beads (0.84 $\mu$m, Spherotech) are added to the imaging buffer and introduced into microfluidic devices. Imaging for bead tracking is performed using a standard CCD camera (Grasshopper3, Point Gray, 1920 × 1200 pixels) with an exposure time of 33 ms. Particle trajectories are determined using a particle tracker algorithm[44] and ImageJ software.[45] Using this analysis framework, bead positions are determined $(x, y)$ and corresponding bead velocities $(v_x, v_y)$ are calculated. Local analysis is used to determine the $x$- and $y$-direction extensional strain rates $(-\dot{\epsilon}_0, \dot{\epsilon}_0)$ by least-squares minimization of

$$\begin{pmatrix} v_x \\ v_y \end{pmatrix} = \begin{pmatrix} -\dot{\epsilon}_0 & 0 \\ 0 & \dot{\epsilon}_0 \end{pmatrix} \begin{pmatrix} x - x_0 \\ y - y_0 \end{pmatrix} \tag{1}$$

where $(x_0, y_0)$ are fitting parameters denoting the stagnation point position and an incompressible fluid is assumed. For bead tracking experiments, >5000 data points spanning the entire image area are analyzed to determine the fluid strain rate $\dot{\epsilon}_0$ as a function of the inlet pressure. In all cases, we find a linear relation between strain rate and input pressure. This process is repeated by using both the top/bottom channels and left/right channels in the cross-slot device as inlets in separate experiments, which ensures symmetry in flow calibration for two-dimensional LAOE experiments.[40] Strain rates in the $x, y$ plane are also determined as a function of the vertical distance ($z$-position) from the glass coverslip surface inside the microfluidic channel, and a parabolic flow profile is observed with respect to the $z$-direction, which is consistent with pressure-driven flow of a Newtonian fluid in the gap between two parallel plates.[7]

**Large Amplitude Oscillatory Extensional Flow.** In order to generate controlled LAOE flows while simultaneously confining single polymers for long times, we used the Stokes trap,[46] which relies on model predictive control (MPC) to precisely position and manipulate single or multiple particles in flow. In brief, the center-of-mass position of a target polymer is determined in real time using fluorescence imaging and image analysis software (LabView). This information is then communicated to the controller that rapidly determines the optimal flow rates within 500 $\mu$s. Based on controller output, the LabView program actuates four independent pressure transducers (Proportion Air) to drive fluid flow in the cross-slot channel at a target strain rate while confining single polymers near the center of the cross-slot. The time required for one iteration of the control loop is approximately 30 ms. Further details of the implementation of the Stokes trap for LAOE can be found elsewhere.[40]

A schematic of the experimental setup is shown in Figure 1. Imaging buffer with fluorescently labeled DNA is introduced into one of the four sample reservoirs, and imaging buffer without DNA is used in the other three reservoirs. Microfluidic adapters (Elveflow) are used to connect fluid reservoirs (1.5 mL Eppendorf tubes, Elveflow) to pressure transducers and the microfluidic flow cell. A custom-fitted cooling jacket is connected to a circulating water bath to precisely control the temperature of the buffer solution. All experiments are conducted isothermally at 22.5 °C.

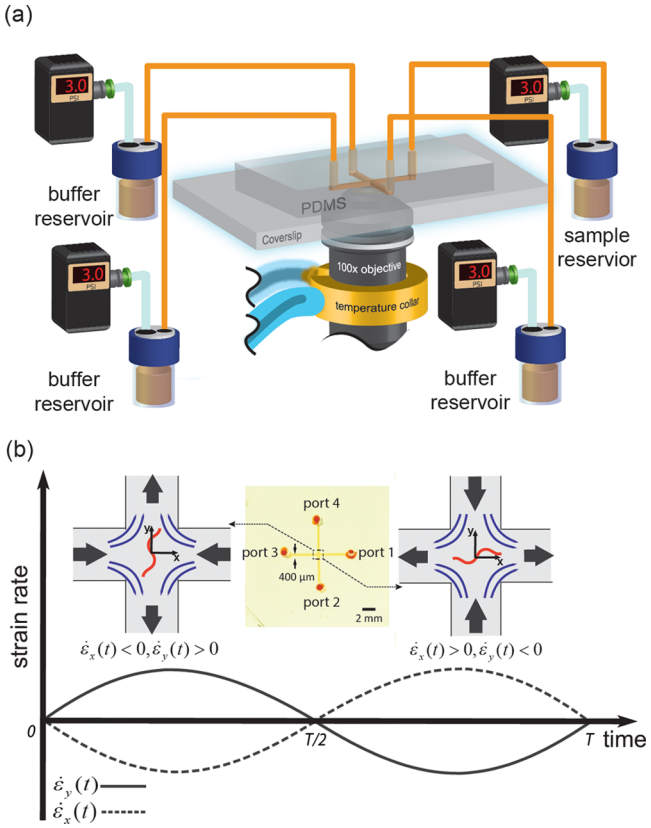


**Figure 1.** Experimental setup for single polymer dynamics in large amplitude oscillatory extension (LAOE). (a) Schematic of the experimental setup for the LAOE experiment. (b) Sinusoidal strain rate input function for one full cycle. Inset: schematics showing the oscillatory extensional flow profile in the microfluidic cross-slot during the first half ($0 < t < T/2$) and second half period ($T/2 < t < T$) of the cycle.

In this work, a sinusoidal strain rate input is implemented to study polymer dynamics in oscillatory extensional flow:

$$\dot{\epsilon}_x(t) = -\dot{\epsilon}_0 \sin\left(\frac{2\pi}{T}t\right) \tag{2}$$

$$\dot{\epsilon}_y(t) = \dot{\epsilon}_0 \sin\left(\frac{2\pi}{T}t\right) \tag{3}$$

where $T$ is the period of the sinusoidal cycle and $\dot{\epsilon}_0$ is the maximum strain rate (Figure 1b). During the first half-cycle for $0 < t < T/2$, the $y$-axis is the extensional axis and the $x$-axis is the compressional axis ($\dot{\epsilon}_x(t) < 0$, $\dot{\epsilon}_y(t) > 0$). During this phase, fluid is introduced into the microfluidic device through ports 1 and 3 via pressure-driven flow, such that the pressure values for ports 1 and 3 are equal ($P_1 = P_3$) and are chosen to achieve the desired strain rate in the channel. During the first half-cycle, ports 2 and 4 are pressured to small pressure values $\delta_2$ and $\delta_4$, wherein the values of $\delta_2$ and $\delta_4$ are obtained from the feedback


DOI: 10.1021/acs.macromol.6b01606
Macromolecules 2016, 49, 8018−8030

controller and are used to effectively confine the target molecule near the center of the cross-slot. Importantly, the magnitudes of $\delta_2$ and $\delta_4$ are much smaller that the pressures applied in ports 1 and 3 to generate the primary flow ($\delta_2 \ll P_{1,3}$ and $\delta_4 \ll P_{1,3}$), such that the application of secondary pressures $\delta_2$ and $\delta_4$ results in negligible changes to the strain rate $\dot{\epsilon}_0$. During the second half-cycle for $T/2 < t < T$, the $y$-axis is the compressional axis and $x$-axis is the extensional axis ($\dot{\epsilon}_x(t) > 0$, $\dot{\epsilon}_y(t) < 0$). During the second half-cycle, the processes essentially reverses compared to the first half-cycle explained above. For all experiments, DNA molecules are imaged for at least $10T$, which corresponds to 10 strain rate cycles. In this work, we focus only on polymer dynamics at long times in oscillatory extensional flow, considering transient dynamics only after the initial transients (during start-up) have died out. In this way, we focus on times $t \gg T$ and $t \gg \tau$, where $\tau$ is the polymer longest relaxation time.[40]

The maximum strain rate $\dot{\epsilon}_0$ is nondimensionalized to define a maximum Weissenberg number $Wi_0 = \dot{\epsilon}_0\tau$, and the cycle period $T$ is nondimensionalized to obtain a Deborah number $De = \tau/T$. We measure $\tau$ by first stretching DNA molecules in steady extensional flow at high strain rates $Wi \gg 1$, followed by cessation of flow. Next, we record the polymer relaxation trajectory after flow cessation, and the maximum projected polymer extension $l(t)$ is tracked over time. This process is repeated for an ensemble of polymer chains. A single-exponential decay function is fit to the average maximum fractional extension squared ($\langle l(t)\rangle/L)^2 = A\exp(-t/\tau) + B$ over the linear elastic regime $l/L < 0.3$, where $L$ is the contour length, $A$ and $B$ are fitting parameters, and $\langle\cdot\rangle$ corresponds to an average quantity. Using this approach, we determined a longest polymer relaxation time $\tau = 4.5 \pm 0.1$ s in 48.5 ± 1 cP imaging buffer, which is consistent with previous single polymer studies.[34−36,47] Single polymer experiments are performed in the range $0 \le Wi \le 10$ and $0 \le De \le 1$ by adjusting the input pressures and strain rate cycle periods. Moreover, only polymers near the center plane of the microchannel (with respect to the $z$-direction) are analyzed. Single polymer images are analyzed using a custom algorithm[48] that allows for clear visualization of polymer conformation and determination of polymer extension and orientation angle.

Particle tracking velocimetry is also used to determine the characteristic response time $\delta t$ for actuating fluid flow in response to a sudden pressure change in the microdevice.[40] In brief, the finite response time arises due to the elasticity of PDMS and flow lines. For the extreme case of a large step pressure impulse of 1.2 psi (yielding a strain rate increase of $\dot{\epsilon} = 1\ s^{-1}$), we found that $\delta t \approx 1$ s. However, LAOE experiments reported in this work are performed with continuously varying pressure changes with small incremental changes that yield much smaller characteristic response times. Nevertheless, we choose cycle time $T$ to be much larger than the maximum characteristic "rise" time $\delta t$ corresponding to a large step input flow rate.

## BROWNIAN DYNAMICS SIMULATIONS

We employed a coarse-grained bead−spring model for polymer chains in dilute solutions to simulate the dynamics of single polymers in LAOE. The details of the BD simulations can be found elsewhere.[31,49] Briefly, the equation of motion for each bead $i$ in an $N$-particle system is described by the Langevin equation. The system is overdamped such that particle momenta relax much faster than particle configurations:

$$m_i\dot{\mathbf{v}}_i = \mathbf{F}_i^{\mathrm{B}} + \mathbf{F}_i^{\mathrm{d}} + \mathbf{F}_i^{\mathrm{s}} \simeq 0 \tag{4}$$

where subscript $i$ denotes bead $i$, $m$ is the mass of bead $i$, $\mathbf{F}_i^{\mathrm{B}}$ is the Brownian force on bead $i$, $\mathbf{F}_i^{\mathrm{d}}$ is the hydrodynamic drag force on bead $i$, and $\mathbf{F}_i^{\mathrm{s}}$ is the net entropic spring force on bead $i$. In this work, we consider only free-draining polymers in the absence of intramolecular hydrodynamic interactions (HI) and excluded volume (EV) interactions. In this model, the drag force on bead $i$ is given by

$$\mathbf{F}_i^{\mathrm{d}} = \zeta\left(\mathbf{v}_i^{\infty} - \frac{\mathrm{d}\mathbf{r}_i}{\mathrm{d}t}\right) \tag{5}$$

where $\zeta$ is the (constant) drag coefficient, $\mathbf{v}_i^{\infty}$ is the solvent velocity at bead $i$, and $\mathbf{r}_i$ is the position vector of bead $i$. We assume a homogeneous velocity field such that $\mathbf{v}_i^{\infty} = \boldsymbol{\kappa}\cdot\mathbf{r}_i$ where $\boldsymbol{\kappa}$ is the velocity gradient tensor. For the time-dependent oscillatory extensional flow studied in this work, the velocity gradient tensor has the form

$$\boldsymbol{\kappa} = \begin{pmatrix} -\dot{\epsilon}_0 \sin\left(\frac{2\pi}{T}t\right) & 0 & 0 \\ 0 & \dot{\epsilon}_0 \sin\left(\frac{2\pi}{T}t\right) & 0 \\ 0 & 0 & 0 \end{pmatrix} \tag{6}$$

where $T$ is the cycle period.

The Brownian forces $\mathbf{F}_i^{\mathrm{B}}$ are defined to satisfy the fluctuation−dissipation theorem such that

$$\langle \mathbf{F}_i^{\mathrm{B}}(t)\rangle = 0 \tag{7}$$

$$\langle \mathbf{F}_i^{\mathrm{B}}(t)\mathbf{F}_j^{\mathrm{B}}(t + \mathrm{d}t)\rangle = 2k_{\mathrm{B}}T\zeta\boldsymbol{\delta}_{ij}\delta(\mathrm{d}t) \simeq \frac{2k_{\mathrm{B}}T\zeta\boldsymbol{\delta}_{ij}}{\mathrm{d}t} \tag{8}$$

where $\boldsymbol{\delta}_{ij}$ is the second-order isotropic tensor, $\delta(t)$ is the Dirac delta function, and $\mathrm{d}t$ is the discrete simulation time step.[50,51] Ignoring bead inertia, eq 4 can now be written as a set of stochastic differential equations for the positions of beads $i = 1$ to $N$:

$$\mathrm{d}\mathbf{r}_i = \left(\boldsymbol{\kappa}\cdot\mathbf{r}_i + \frac{1}{\zeta}\mathbf{F}_i^{\mathrm{s}}\right)\mathrm{d}t + \sqrt{\frac{2k_{\mathrm{B}}T}{\zeta}}\,\mathrm{d}\mathbf{W}_i \tag{9}$$

For each of the $N$ equations, $\mathrm{d}\mathbf{W}_i$ represents an independent three-dimensional Wiener process[50] whose value is represented as the product of $\sqrt{\mathrm{d}t}$ and a randomly distributed Gaussian vector $\mathbf{n}_i$ with zero mean and unit variance. Equation 9 is nondimensionalized using a characteristic time scale $t_s = \zeta/4H_s$, length scale $l_s = \sqrt{kT/H_s}$, and force scale $F_s = \sqrt{kTH_s}$, where $H_s = 3kT/N_{k,s}b_k^2$ is the Hookean spring constant.[52] The Kuhn step size is $b_k$, the number of Kuhn steps per spring is $N_{k,s}$, and the total number of Kuhn steps in the polymer is $N_{k,\mathrm{tot}} = (N-1)N_{k,s}$. The internal configuration of a bead−spring polymer chain is described by a series of connector vectors $\mathbf{Q}_i = \mathbf{r}_{i+1} - \mathbf{r}_i$ where $i$ ranges from 1 to $N-1$. Equation 9 is recast into dimensionless form in terms of connector vectors $\mathbf{Q}_i$ as

$$\mathrm{d}\mathbf{Q}_i = \left[Pe(\boldsymbol{\kappa}\cdot\mathbf{Q}_i) + \frac{1}{4}(\mathbf{F}_{i-1}^{\mathrm{s}} - 2\mathbf{F}_i^{\mathrm{s}} + \mathbf{F}_{i+1}^{\mathrm{s}})\right]\mathrm{d}t + \frac{1}{2}(\mathrm{d}\mathbf{W}_{i+1} - \mathrm{d}\mathbf{W}_i) \tag{10}$$

where $\boldsymbol{\kappa} = \sin(2\pi\tilde{t}/\tilde{T})(-\boldsymbol{\delta}_{m1}\boldsymbol{\delta}_{n1} + \boldsymbol{\delta}_{m2}\boldsymbol{\delta}_{n2})$, the bead Péclet number is $Pe = \dot{\epsilon}_0\zeta/4H_s$, and $\tilde{t}$ and $\tilde{T}$ are dimensionless time and the dimensionless cycle period, respectively. The maximum flow strength is given by the Weissenberg number $Wi_0 = Pe\tilde{\tau}$, and the dimensionless cycle frequency is given by the Deborah number $De = \tilde{\tau}/\tilde{T}$, where $\tilde{\tau}$ is the dimensionless longest relaxation time for the bead−spring chain. We used the Marko−Siggia entropic force relation between two consecutive beads in the bead−spring chain such that[53]


DOI: 10.1021/acs.macromol.6b01606
Macromolecules 2016, 49, 8018−8030

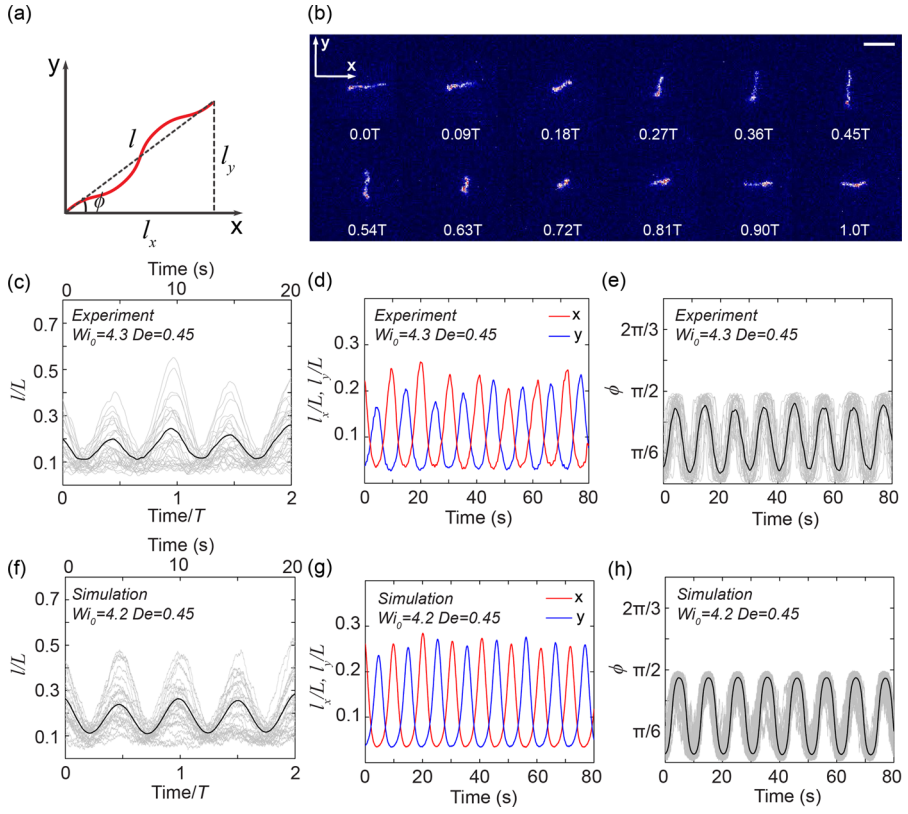


**Figure 2.** Single polymer dynamics in large amplitude oscillatory extension (LAOE). (a) The total extension in the $x-y$ plane is $l$, the $x$-direction projected extension is $l_x$, the $y$-direction projected extension is $l_y$, and the orientation angle is $\phi$. (b) Snapshots of a single DNA molecule over one LAOE cycle (scale bar = 5 $\mu$m). (c) Experimental trajectories of fractional projected extension $l/L$ at $Wi_0 = 4.3$ and $De = 0.45$. Here, 34 individual experimental trajectories (gray) are used to calculate the ensemble average extension $l/L$ (black). (d) Experimental trajectories of $x$-direction fractional projected extension $l_x/L$ (red) and $y$-direction fractional projected extension $l_y/l$ (blue). (f) Experimental trajectories of polymer orientation angle $\phi$. Here, 34 individual experimental trajectories (gray) are used to calculate the ensemble average angle $\phi$ (black). (f–h) Results from BD simulations showing $l/L$, $l_x/L$, $l_y/L$, and $\phi$ corresponding to the experimental data in parts c–e, respectively. For BD simulations, 250 polymer chains are included in the ensemble.

$$\mathbf{F}_i^s = \frac{kT}{b_k}\left[\frac{1}{2}\frac{1}{(1-(Q/Q_0))^2} - \frac{1}{2} + \frac{2Q}{Q_0}\right]\frac{\mathbf{Q}_i}{Q_0} \tag{11}$$

where $Q$ is the scalar magnitude of the connector vector $\mathbf{Q}_i$ and $Q_0$ is the maximum extensibility of a spring given by $Q_0 = N_{k,s}b_k$. The stochastic differential equations given by eq 10 were solved using a semi-implicit predictor–corrector algorithm.[52] Polymer chains in the simulated ensemble are allowed to equilibriate for $10\tilde{\tau}$ before initiating oscillatory extensional flow in order to ensure random conformational distributions. For this work, we use $N_s = 10$ and $N_{k,s} = 15$, which is similar to prior work on $\lambda$-DNA.[54,55]

## RESULTS AND DISCUSSION

**Transient Dynamics in LAOE.** We began the experiment by studying the dynamics of single $\lambda$-DNA molecules in LAOE (Figure 2). Single chain dynamics are observed and analyzed in the $x$, $y$ plane, wherein the $x$- and $y$-directions continuously switch roles as the extensional and compressional axes in the oscillatory flow field, as defined by eqs 2 and 3. Single molecule images are analyzed using the quantities defined in Figure 2a, and individual polymer backbones are tracked using custom image analysis code (Methods). Using this approach, we directly determine the maximum (total) polymer extension in the $x-y$ plane $l$, the $x$-direction projected extension $l_x$, and the $y$-direction projected extension $l_y$. These quantities can be converted to fractional extension by normalizing with the polymer contour length $L$. The orientation angle $\phi$ is defined as $\phi = \tan^{-1}(l_y/l_x)$, and for the purposes of this analysis, the directionality of $l_x$ and $l_y$ is not taken into consideration such that the value of $\phi$ ranges from 0 to $\pi/2$.

Representative images of single polymers in a full LAOE cycle at $Wi_0 = 4.3$ and $De = 0.45$ are shown as a series of single molecule snapshots in Figure 2b. Under these conditions, the flow strength $Wi_0 > 1$, which suggests that polymers should be stretched to high degrees of extension, at least in the context of steady extensional flow at $De = 0$. However, for these conditions, the cycle time is approximately twice the longest polymer relaxation time ($De = 0.45$), which means that the transient polymer extension will be a competition between the rate of stretching and duration of each cycle. Indeed, we observe that single polymers indeed stretch beyond equilibrium coil dimensions at $Wi_0 = 4.3$ and $De = 0.45$; however, the maximum stretch in LAOE ($l_{max}/L \approx 0.3$) appears to be less than that observed under steady extensional flow at $Wi_0 = 4.3$ and $De = 0$ ($l_{max}/L \approx 0.8$, as reported in Figure 5 and in prior work[34]). The interplay between $Wi$ and $De$ in determining chain dynamics is explored in more detail throughout this article, though to begin this discussion, it is instructive to consider transient polymer dynamics during a characteristic LAOE cycle.



DOI: 10.1021/acs.macromol.6b01606
Macromolecules 2016, 49, 8018–8030

Snapshots of a single polymer undergoing one complete LAOE cycle are shown in Figure 2b, and the corresponding ensemble average transient polymer stretch ($l(t)/L$, $l_x(t)/L$, $l_y(t)/L$) and the transient orientation angle $\phi(t)$ at $Wi_0 = 4.3$ and $De = 0.45$ are shown in Figures 2c–e. Here, the polymer is exposed to a transient cycle of LAOE defined by strain rates shown in Figure 1b. On the basis of these data, we can describe the dynamic behavior of a single polymer chain in steady LAOE by a characteristic periodic cycle. At the start of the cycle at $t = 0T$, a polymer chain begins in a nonequilibrium stretched state in the $x$-direction because the $x$-axis served as the prior extensional axis for $t^- < 0$. At time $t = 0$, peaks are observed for both $l$ and $l_x$, and valleys are seen for the $l_y$ trajectory and the $\phi$ trajectory. Intuitively, as the majority of the polymer stretch appears in the $x$-direction, the $y$-direction stretch $l_y$ is essentially zero. Next, in the first quarter of the LAOE cycle ($0T < t < 0.25T$), the $y$-axis is the extensional axis and the $x$-axis is the compressional axis. The strain rate in the $y$-direction increases, which results in the polymer chain compressing in the $x$-direction while rotating toward the $y$-direction. At the same time, the polymer begins to stretch along the $y$-axis, which is reflected in an increase in the values of $l_y$ and $\phi$ with a corresponding decrease in $l_x$.

In the second quarter of the LAOE cycle ($0.25T < t < 0.5T$), the $y$-axis remains as the extensional axis, but the strain rate in the $y$-direction begins to decrease. Passing the maximum strain rate value $\dot{\epsilon}_y$ at $t = 0.25T$, the polymer chain continues to be stretched along the $y$-direction, albeit with a small amount of retraction. Hence, at $t = 0.5T$, the maximum polymer stretch occurs along the $y$-axis with essentially no stretch at the $x$-direction. The orientation angle $\phi$ continues to increase from approximately $\pi/5$ to a peak close to $\pi/2$. In the third quarter of the cycle ($0.5T < t < 0.75T$), the flow switches direction such that the $x$-axis is the new extensional axis and the $y$-axis is the new compressional axis. The dynamic cycle essentially follows the reverse process described in the first half-cycle, albeit with the roles of the $x$- and $y$-directions switched. At $t = 0.5T$, the polymer chain is stretched along the $y$-axis, but at the cycle proceeds, the polymer begins to compress along the $y$-direction and rotates toward the $x$-axis. The cycle proceeds for the final quarter ($0.75T < t < T$) until the end of cycle at $t = T$, where polymer chain is again stretched along the $x$-axis, and the cycle begins anew.

To complement single molecule experiments, we also studied the dynamics of single polymers in LAOE using free-draining Brownian dynamics simulations. Simulation results for transient trajectories of $l(t)/L$, $l_x(t)/L$, $l_y(t)/L$, and the transient orientation angle $\phi(t)$ at $Wi_0 = 4.2$ and $De = 0.45$ are shown in Figures 2f–h. Overall, we observe good agreement between the experiments and simulation trajectories for transient polymer dynamics under these conditions. In prior work, we also investiagated the role of intramolecular hydrodynamic interactions (HI) and excluded volume (EV) interactions in describing the dynamics of $\lambda$-DNA in LAOE in the range $0 \leq Wi_0 \leq 10$ and $0 \leq De \leq 2$.[40] In general, we found that inclusion of HI and EV into the BD simulations results in fairly minor differences in describing chain dynamics compared to free-draining simulations. Moreover, the role of HI and EV lessens even further at low $De$, wherein polymer chains are able to unravel to high extensions during a cycle and intramolecular interactions are relatively weak.[40] For these reasons, we focus our attention on free-draining BD simulations in this work.

As shown in Figure 2, the dynamic trajectories of $l$, $l_x$, $l_y$, and $\phi$ show high degrees of periodicity. We further investigated the periodic cycle of polymer motion by examining the power spectral density (PSD) of the $x$–$y$ plane extension $l$ and the orientation angle $\phi$ (Figure 3). By observing the power of a

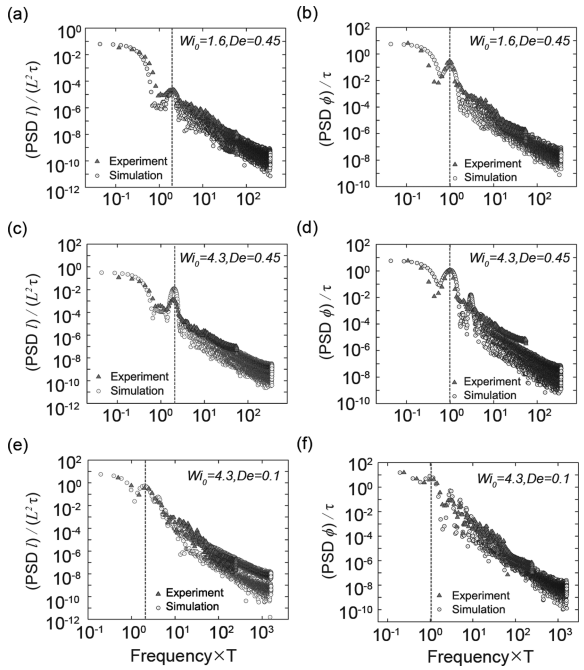


**Figure 3.** Power spectral densities (PSDs) of transient quantities in oscillatory extension from both experiments and simulations. (a), (c), and (e) show PSDs for polymer extension $l$ in the $x$–$y$ plane at different combinations of $Wi_0$ and $De$. (b), (d), and (f) show PSDs of polymer orientation angle $\phi$ in LAOE at different combinations of $Wi_0$ and $De$.

fluctuating signal in frequency space, the underlying time and frequency dependencies can be conveniently characterized. The PSD is defined as the Fourier transform of the autocorrelation function of a quantity (or cross-correlation of two quantities).[30−33,37,54,56] The autocorrelation function of a real-valued, integrable fluctuating quantity $x(t)$ is defined as

$$C_{x,x}(\lambda) = \langle x(t)x(t+\lambda)\rangle \tag{12}$$

where $t$ denotes time, $\lambda$ is the offset time and $\langle\cdot\rangle$ denotes a time-averaged quantity. The PSD of $x(t)$ is given by

$$P(f) = \int_{-\infty}^{\infty} C_{x,x}(\lambda)\mathrm{e}^{-2i\pi f\lambda}\,\mathrm{d}\lambda \tag{13}$$

where $P$ is power, $f$ is frequency, and $i$ is the imaginary unit. Here, the data are multiplied by a Welch window before computing the Fourier transform using a fast Fourier transform (FFT) algorithm.[56] For both experiments and simulations, the PSD of the projected extension $l$ is nondimensionalized by the quantity $L^2\tau$, where $L$ is the contour length and $\tau$ is the longest polymer relaxation time. The PSD for the orientation angle $\phi$ is nondimensionalized by $\tau$, and frequency is nondimensionalized by the cycle period time $T$.

PSDs of polymer extension $l$ and orientation angle $\phi$ from experiments and simulations are shown in Figure 3, where the data correspond to two different $Wi_0$ (at constant $De$) and two different $De$ (at constant $Wi_0$). From a broad perspective, we observe good agreement for PSDs between experiments and


DOI: 10.1021/acs.macromol.6b01606
Macromolecules 2016, 49, 8018−8030

simulations. For PSDs of polymer extension $l$ (Figures 3a,c,e), distinct peaks are observed at $fT = 2$, which corresponds to a frequency equal to the inverse half-cycle time $(T/2)^{-1}$. These data indicate that polymer chains reach their maximum extension in the $x-y$ plane exactly twice in one LAOE cycle, which includes polymer chain stretching along the $x$-axis and $y$-axis in the cycle discussed above. We observe this characteristic periodicity across a wide range of flow strength $Wi_0$ and probing frequency $De$. Figures 3b,d,f show the PSDs of the orientation angle $\phi$ from experiments and simulations. In terms of orientation angle, peaks in the PSD are observed at $fT = 1$, which corresponds to a frequency equal to the inverse cycle time $T^{-1}$. PSDs of $\phi$ imply that polymer chains can fully rotate exactly once within one LAOE cycle from $\phi = 0$ to $\phi = \pi/2$ and back to $\phi = 0$ again, at least across the range of $Wi_0$ and $De$ considered in these data. Interestingly, these results show that the characteristic periodic dynamics of polymers in LAOE can emerge even under relatively weak flow strength ($Wi_0 = 1.6$), though the precise dynamics will depend on the specific values of $Wi_0$ and $De$.

To further understand the coupled dynamics between $l_x$ and $l_y$ in the $x-y$ plane, we determined the cross-correlation function for fluctuations in the projected extensions $l_x$ and $l_y$ (Figure 4). Here, we define fluctuations in the projected

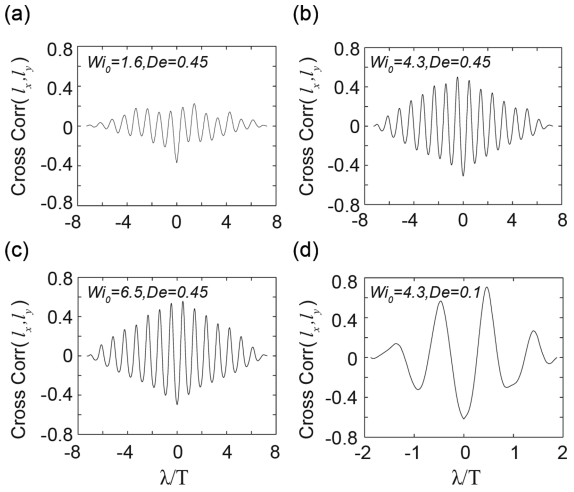


**Figure 4.** Cross-correlations of $x$-direction projected extension $l_x$ and $y$-direction projected extension $l_y$ from single polymer LAOE experiments at (a) $Wi_0 = 1.6$ and $De = 0.45$, (b) $Wi_0 = 4.3$ and $De = 0.45$, (c) $Wi_0 = 6.5$ and $De = 0.45$, and (d) $Wi_0 = 4.3$ and $De = 0.1$.

extensions as the mean value subtracted from the instantaneous value such that $l'_x(t) = l_x(t) - \langle l_x \rangle$ and $l'_y(t) = l_y(t) - \langle l_y \rangle$, where $\langle \cdot \rangle$ denotes a time-averaged quantity. The cross-correlation function $C_{l'_x\, l'_y}$ is given by

$$C_{l'_x,l'_y}(\lambda) = \frac{\langle l'_x(t) l'_y(t+\lambda)\rangle}{\sqrt{\langle l'^2_x(t)\rangle \langle l'^2_y(t)\rangle}} \equiv \frac{\int_{-\infty}^{\infty} l'_x(t) l'_y(t+\lambda)\, dt}{\langle l'^2_x(t)\rangle \langle l'^2_y(t)\rangle} \tag{14}$$

where the function $C_{l'_x\, l'_y}$ is normalized by the product of the mean-squared fluctutations in extension in the $x$- and $y$-directions. The cycle period $T$ is used to nondimensionalize the offset time $\lambda$. Using this approach, we observe some similarities in cross-correlations for these data, at least in the range of $Wi$ and $De$ considered here. First, the results show that all cross-correlations defined by $C_{l'_x,l'_y}$ are symmetric with respect to $\lambda = 0$. Moreover, the cross-correlation analysis reveals that the fluctuations in polymer stretch in the $x$- and $y$-directions are esssentially perfectly anticorrelated. At zero lag ($\lambda = 0T$), the quantities $l'_x$ and $l'_y$ are negatively correlated, suggesting that peaks in $l_x$ correspond to valleys in $l_y$, which is consistent with the general behavior shown in Figure 2. As the lag increases to $\lambda = T/4$, zero correlation is observed between $l'_x$ and $l'_y$, which suggests that polymer stretch in the $x$- and $y$-directions becomes completely uncorrelated in one-quarter cycle time $(T/4)$ relative to zero lag. In fact, for any $(\lambda/T)_n = \pm\left(\frac{n}{2} + \frac{1}{4}\right)$, $n \in \mathbb{Z}$, zero correlation is observed, which reflects the underlying periodic nature of the LAOE flow. As the lag further increases to $\lambda = T/2$, the quantities $l'_x$ and $l'_y$ are perfectly correlated, which is again consistent with the dynamic behavior shown in Figures 2d and 2g. In order to interpret the cross-correlation function, consider the behavior on either side of zero lag. Moving forward in lag from from $\lambda = 0$ to $\lambda = T/4$, the correlation is negative, suggesting that future positive fluctuations in $y$-direction extension are correlated with negative fluctuations in the $x$-direction extension. For example, stretching along the $y$-axis implies that the polymer chain compresses along the $x$-axis. Alternatively, this behavior similarly implies that future negative fluctuations in $y$-direction extension are correlated with positive fluctuations in the $x$-direction extension. For negative time lags, similar arguments can be made; for example, prior negative fluctuations in $l_y$ give rise to stretching in the $x$-direction. Taken together, this dynamic behavior is consistent with a time-dependent oscillatory process as shown in Figure 2.

**Average Transient Extension in LAOE.** In addition to transient dynamics, we also studied the average polymer extension in oscillatory extensional flow (Figure 5). Unlike

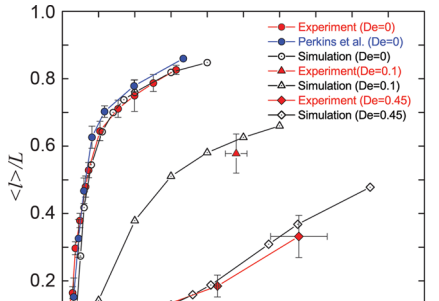


**Figure 5.** Average fractional projected extension $\langle l \rangle / L$ as a function of $Wi_0$ and $De$, including steady extensional flow ($De = 0$) and periodic extensional flow ($De > 0$). Experimental results are compared to BD simulations of $\lambda$-DNA.

steady extensional flow ($De = 0$), polymer chains do not exhibit a stable steady-state extension in LAOE. Rather, the long time dynamics exhibit a periodic transient motion of unsteady polymer stretching. Nevertheless, we can determine the average polymer extension in the $x-y$ plane $\langle l \rangle$ by averaging transient polymer extension $l(t)$ trajectories over long times in experiments or simulations.[37] As noted earlier, in this work we only consider dynamic behavior after the initial start-up phase of LAOE ($t \gg \tau$ and $t \gg T$), and therefore we only


DOI: 10.1021/acs.macromol.6b01606
Macromolecules 2016, 49, 8018−8030

consider the dynamic behavior after the initial transients have died out. The average fractional steady-state extension $\langle l \rangle / L$ as a function of $Wi_0$ and $De$ is shown in Figure 5. For experimental data, >30 individual DNA molecules are analyzed at each $Wi_0$ and $De$. In all cases, single polymers are confined near the stagnation point using the Stokes trap in order to achieve arbitrarily long residence times.

We began the experiment by studying dynamics in steady extensional flow, which corresponds to $De = 0$ in Figure 5. Our experimental and simulation results agree well with previously reported data on steady-state extension of $\lambda$-DNA in steady planar extensional flow.[34,55] We next studied average polymer extension in oscillatory extension by increasing the frequency to $De = 0.1$. In the limit of small $0 < De < 1$, the dynamic behavior of polymers can be referred to as quasi-steady. Under quasi-steady-state conditions, the oscillatory period $T$ is larger than the longest relaxation time $\tau$ such that $De = \tau/T < 1$, which means that a polymer generally has sufficient time to respond to flow during a cycle (relative to the longest relaxation time). Interestingly, at $De = 0.1$, we observe that the average transient extension is much smaller compared to steady extensional flow at $De = 0$. Physically, the presence of flow oscillations decreases the average polymer extension in each phase of the cycle. Upon further increasing the frequency to $De = 0.45$, the average transient extension at equivalent $Wi_0$ further decreases compared to average chain extension at $De = 0$.

The average polymer extension in oscillatory extensional flow was characterized over a wide range of $Wi_0$ and $De$ using BD simulations (Figure 6). As shown in Figure 6a, the average extension curves from BD simulations follow the same trends as discussed above, such that the average polymer stretch

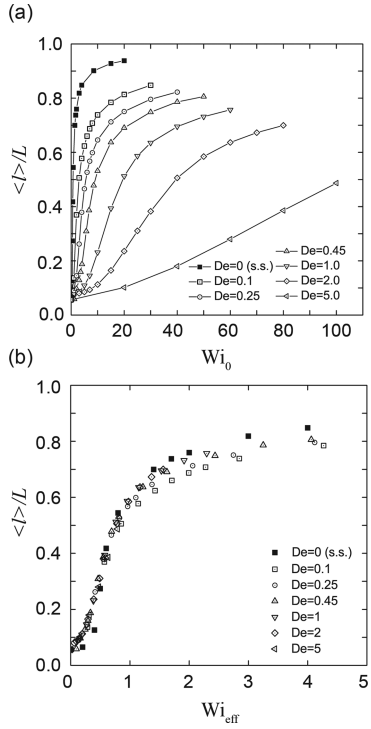


**Figure 6.** Average transient polymer extension in oscillatory extensional flow from BD simulations. (a) Average fractional extension $\langle l \rangle / L$ over a wide range of $Wi_0$ and $De$. (b) Master curve for average transient fractional extension in oscillatory extensional flow by plotting $\langle l \rangle / L$ as a function of $Wi_{eff}$.

gradually decreases upon increasing $De$. In considering Figure 6a, a question arises: can the average extension curves in LAOE be recast into a master curve? To address this question, we derived an analytical expression for the transient polymer extension in oscillatory extensional flow using a Hookean dumbbell model. The rheological equation of state for a suspension of elastic single-mode Hookean dumbbells is[57]

$$\boldsymbol{\tau}_p + \lambda_H \boldsymbol{\tau}_{p(1)} = -nkT\lambda_H \dot{\boldsymbol{\gamma}} \tag{15}$$

where $\boldsymbol{\tau}_p$ is the polymer contribution to the total stress, $\dot{\boldsymbol{\gamma}}$ is the deformation tensor, $\lambda_H$ is the relaxation time for a Hookean dumbbell, and the subscript $(1)$ denotes the operation of codeformational differentiation.[57] For oscillatory extension, the deformation tensor $\dot{\boldsymbol{\gamma}}$ can be taken as the velocity gradient tensor $\boldsymbol{\kappa}$ given by eq 6. Stress is nondimensionalized by the quantity $nkT$, where $n$ is the number density of polymers, and the deformation rate is nondimensionalized by $\lambda_H$. In this way, the following dimensionless differential equations are obtained from eq 15:

$$\left(1 + \lambda_H \frac{d}{dt}\right)\tau_{xx} + Wi_0 \sin\left(\frac{2\pi}{T}t\right)\tau_{xx} = Wi_0 \sin\left(\frac{2\pi}{T}t\right) \tag{16}$$

$$\left(1 + \lambda_H \frac{d}{dt}\right)\tau_{yy} - Wi_0 \sin\left(\frac{2\pi}{T}t\right)\tau_{yy} = -Wi_0 \sin\left(\frac{2\pi}{T}t\right) \tag{17}$$

Given an appropriate set of initial conditions, $\tau_{xx}$ and $\tau_{yy}$ can be solved analytically for Hookean dumbbells in oscillatory extensional flow, albeit in the context of low $Wi_0$. Moreover, the fractional extension in the $x-y$ plane $l(t)$ can be determined using the relation

$$\frac{l}{L} = \frac{R_{eq}}{L}\sqrt{1 - \frac{\tau_{xx} + \tau_{yy}}{3}} \tag{18}$$

where $R_{eq}$ is equilibrium end-to-end distance and $L$ is the contour length. In this way, eqs 16 and 17 can be solved to yield the following expressions for transient fractional extension $l(t)/L$ for a Hookean dumbbell:

$$\frac{l(t)}{L} = \frac{R_{eq}}{L}\Big[1 - \frac{1}{\lambda_H}\exp(A(t))\int_0^t Wi_0 \sin\left(\frac{2\pi De}{\lambda_H}t'\right)\exp(-A(t'))\,dt' + \frac{1}{\lambda_H}\exp(-B(t))\int_0^t Wi_0 \sin\left(\frac{2\pi De}{\lambda_H}t'\right)\exp(B(t'))\,dt'\Big]^{1/2} \tag{19}$$

where

$$A(t) = \frac{\frac{Wi_0\lambda_H}{De}\cos\left(\frac{2\pi De}{\lambda_H}t\right) - 2\pi t}{2\lambda_H\pi};$$

$$B(t) = \frac{\frac{Wi_0\lambda_H}{De}\cos\left(\frac{2\pi De}{\lambda_H}t\right) + 2\pi t}{2\lambda_H\pi} \tag{20}$$

The average polymer extension $\langle l \rangle / L$ at any $Wi_0$ and $De$ is then calculated numerically by integrating eq 19 over at least five cycles in oscillatory extensional flow at long times after the initial transients have died out. Of course, the Hookean dumbbell model can only be used to quantitatively determine the linear flow response of polymers in extensional flow.[57] Nevertheless, this model can be used to define an approximate critical flow strength $Wi_{0,crit}$ for a given $De$ at which the behavior transitions from a linear to nonlinear response in oscillatory extensional flow. In examining the steady-state polymer



DOI: 10.1021/acs.macromol.6b01606
Macromolecules 2016, 49, 8018−8030

extension at $De = 0$, the coil−stretch transition occurs at $Wi_{0,crit} \approx 0.5$, for which the average fractional extension is $\langle l \rangle / L \approx 1/2$. Using this logic, we define the transition from linear to nonlinear behavior to occur at a critical Weissenberg number $Wi_{0,crit}$ at which the average polymer extension $\langle l \rangle / L = 0.5$. Interestingly, using these criteria, we found that the critical Weissenberg number $Wi_{0,crit}$ scales linearly with $De$ over a wide range of $De$ such that $Wi_{0,crit} \propto kDe + 1$, where $k$ is a numerical constant. One aspect of this definition should be noted before proceeding. This definition of $Wi_{0,crit}$ is appropriate for a linear model because the polymer extension diverges at $Wi > 1$ for a Hookean dumbbell in steady planar extensional flow. For this reason, it is physically reasonable to define the linear to nonlinear transition in terms of average polymer extension, rather than an arbitrary critical flow strength. Indeed, the following section shows that this definition is consistent with an alternative (albeit similar) definition of $Wi_{0,crit}$ based on an effective Weissenberg number $Wi_{eff}$ in oscillatory extension. In any event, we emphasize that the Hookean dumbbell model is primarily used to motivate a functional form for an effective Weissenberg number $Wi_{eff}$ in oscillatory extensional flow.

On the basis of these results, we can define an effective Weissenberg number $Wi_{eff}$ for oscillatory extensional flow:

$$Wi_{eff} = \frac{Wi_0}{kDe + 1} \tag{21}$$

where $k$ is a numerical constant ($k = 17.4$ for the Hookean dumbbell model). Using the definition of $Wi_{eff}$ in eq 21, we replotted the average polymer extension data from multimode BD simulations in Figure 6a as a function of $Wi_{eff}$, and the results are shown in Figure 6b. Remarkably, all average extension curves in oscillatory extensional flow collapse onto a single master flow curve when plotted against $Wi_{eff}$, where $k = 25.1$ gives the best fit to collapse data from BD simulation results. We conjecture that the small difference in the numerical constant $k$ between Hookean dummbell model and multimode simulations is due to the inclusion of finite extensibility and multiple modes in the BD simulations.

Finally, the effective Weissenberg number $Wi_{eff}$ in eq 21 can be physically motivated by considering the amount of fluid strain $\epsilon_{T/2}$ applied during a half-cycle:

$$\epsilon_{T/2} = \int_0^{T/2} \dot{\epsilon}_0 \sin\left(\frac{2\pi}{T}t\right) dt = \dot{\epsilon}_0 \frac{T}{\pi} \tag{22}$$

Of course, the total fluid strain applied during a full cycle ($0 < t < T$) is exactly zero ($\epsilon_T = 0$). Thus, the strain in a half-cycle $\epsilon_{T/2}$ can be rewritten as

$$\epsilon_{T/2} = \frac{Wi_0}{\pi De} \tag{23}$$

Hence, the inverse scaling behavior of $Wi_{eff}$ and $De$ in eq 21 indicates an interplay between the flow strength $Wi_0$ and cycle frequency $De$ that ultimately determines the amount of accumulated fluid strain during a half-cycle in oscillatory extensional flow. Physically, one would expect that larger amounts of fluid strain $\epsilon_{T/2}$ will result in larger polymer deformations during an LAOE cycle. Indeed, this is observed in our experiments.

**Single Polymer Dynamics in Pipkin Space.** Dynamic behavior in LAOE can be described by a two-dimensional space known as Pipkin space, which is defined by flow strength $Wi_0$ and frequency $De$.[58] Figure 7 shows a sketch of polymer behavior in oscillatory extensional flow in the context of Pipkin space. Under these conditions, polymer dynamics can be generally classified by six regimes: (1) Regime I: linear, steady-state behavior for $Wi_0 < Wi_{0,crit}$ and $De = 0$; (2) Regime II: linear, quasi-steady-state behavior for $Wi_0 < Wi_{0,crit}$ and $De < 1$; (3) Regime III: linear, unsteady behavior at $Wi_0 < Wi_{0,crit}$ and $De > 1$; (4) Regime IV: nonlinear, steady-state behavior at $Wi_0 > Wi_{0,crit}$ and $De = 0$; (5) Regime V: nonlinear, quasi-steady-state behavior for $Wi_0 > Wi_{0,crit}$ and $De < 1$; and (6) Regime VI: nonlinear, unsteady behavior at $Wi_0 > Wi_{0,crit}$ and $De > 1$. Steady extensional flow corresponds to zero frequency or infinite cycle times ($De = 0$), denoted by Regimes I and IV (shaded black) on the far left side of plot in Figure 7. At $De = 0$, the critical Weissenberg number at the coil−stretch transition (CST) is $Wi^{SS}_{0,crit} = 0.5$ from kinetic theory,[59] which is in good agreement with experimental observations.[34] In constructing the dynamic phase diagram for oscillatory extensional flow, a key question arises: what defines the critical flow strength $Wi_{0,crit}$ at the boundary between the linear and nonlinear regimes?

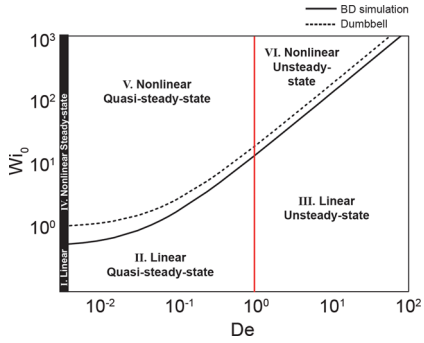


**Figure 7.** Average polymer stretching dynamics in oscillatory extensional flow as visualized in the context of Pipkin space, which is defined in the two-dimensional space of $Wi_0$ and $De$. Here, we identify six diffent regimes, with the transition between linear and nonlinear behavior predicted from BD simulations (solid line) and a Hookean dumbbell model (dashed line).

We determined the critical Weissenberg number at the linear to nonlinear transition $Wi^{LAOE}_{0,crit}$ using multimode BD simulations and the effective Weissenberg number $Wi_{eff}$ defined in eq 21. In this way, the critical $Wi_{0,crit}$ in oscillatory extension can be related to the critical Weissenberg number in steady extensional flow $Wi^{SS}_{0,crit}$ by the relation

$$Wi^{LAOE}_{0,crit}(De) = Wi^{SS}_{0,crit}(kDe + 1) \tag{24}$$

In eq 24, the critical flow strength is formally defined to occur at $Wi_{eff} = 0.5$, which is in good agreement with the master curve shown in Figure 6b. Using this framework, the dynamic behavior of polymers in oscillatory extensional flow can be schematically illustrated in Pipkin space, as shown in Figure 7. Here, the linear regime corresponds to the linear portion of the average flow extension curves in Figure 6a. In this regime, polymer chains are only slightly perturbed beyond equilibrium. Upon increasing the flow strength $Wi_0$ into the nonlinear regime, polymer chains can be deformed into highly stretched states depending on the $De$. For $Wi_0 > Wi^{LAOE}_{0,crit}$ and $De < 1$, quasi-steady-state conditions such that the cycle times are longer than the polymer relaxation time, which results in highly stretched conformations in each half-cycle. Upon increasing the $De$ further at high $Wi_0 > Wi^{LAOE}_{0,crit}$, complex chain dynamics are expected to be observed under highly unsteady conditions.



DOI: 10.1021/acs.macromol.6b01606
Macromolecules 2016, 49, 8018−8030

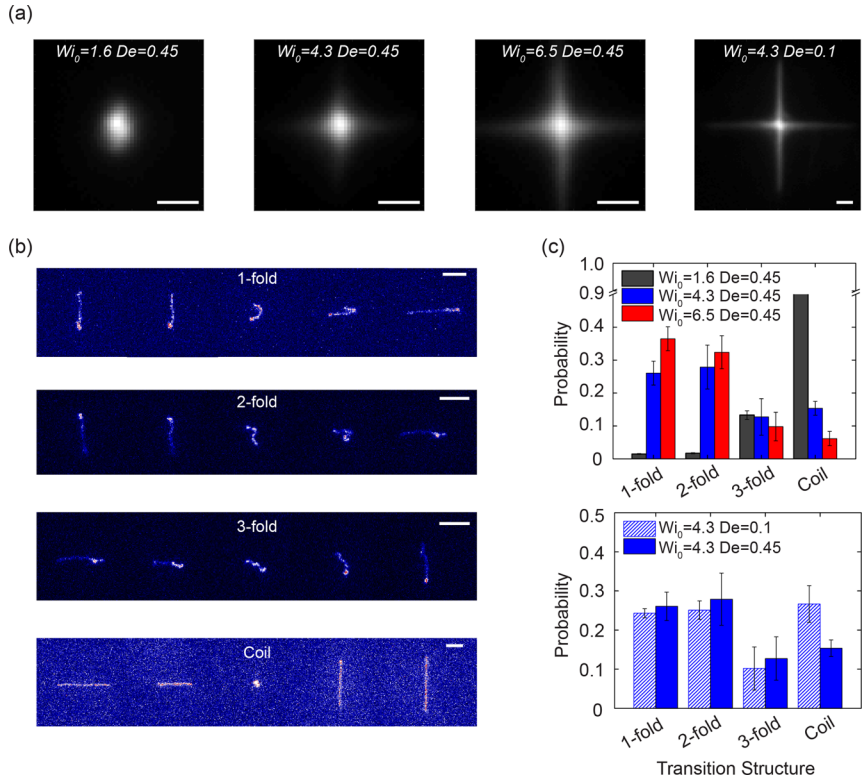


**Figure 8.** Dynamic polymer conformations in oscillatory extension. (a) Average conformational space for an ensemble of single DNA molecules as a function of $Wi_0$ and frequency $De$. For these data, fluorescence images were superimposed for a series of experiments at a particular $Wi_0$ and $De$, and the center-of-mass of the polymer was centered at the origin. Scale bar = 2 $\mu$m. (b) Single molecule snapshots showing different transition conformational structures observed during a switch in the extensional/compressional axes. Different apparent buckling structures are observed. The time between each single polymer snapshot is $T/10$. Scale bar = 5 $\mu$m. (c) Histograms showing probabilities of different transition structures as a function of $Wi_0$ and $De$ above the critical Weissenberg number $Wi_{0,crit}^{LAOE}$.

These results can be further analyzed to determine the amount of fluid strain required to drive a polymer from the linear to nonlinear state in LAOE, which can be approximated as the strain in a half-cycle at $Wi_{eff} = 0.5$. We found that the strain required to transition from the linear to nonlinear regime during a half-cycle is $\epsilon \sim 4$. Interestingly, this value is close to the amount of strain required to uncoil a polymer molecule before reaching a steady state stress or extension ($\epsilon \sim 2-6$) as determined using a filament stretching rheometer (FSR).[20] In addition, the linear to nonlinear transition predicted from single polymer LAOE is very similar to the linear and nonlinear rheological features of wormlike micelle solutions determined by LAOS, which is a physical process that includes the breakage and re-forming of an entangled physical network.[60] From this perspective, there appear to be similarities in the underlying physics governing the linear to nonlinear transitions for complex fluids in oscillatory flows, despite the fact that these materials are quite different in nature.

**Dynamic Polymer Conformations in LAOE.** We further investigated the dynamic conformations of single polymers in LAOE (Figure 8). We began by studying the average conformational phase space of single polymers experiments as a function of $Wi_0$ and $De$, as shown in Figure 8a. Here, we superimposed single molecule fluorescence images across all experiments at a particular $Wi_0$ and $De$, such that the center-of-mass of the polymer was fixed at the origin for all images.[33] In this way, the dynamic conformational phase space becomes visually apparent for nonequilibrium flows. We observe several trends in these data. When the flow strength $Wi_0$ (at a frequency $De$) is below the critical Weissenberg number $Wi_{0,crit}^{LAOE}(De)$, the conformational space for single polymers appears as an isotropic blob. This behavior occurs for the case of $Wi_0 = 1.6$ and $De = 0.45$, wherein critical Weissenberg number $Wi_{0,crit}^{LAOE}(De) \approx 6.1 \gg Wi_0 = 1.6$. These data indicate that polymer chains (on average) experience minor deformations and perturbations from an equilibrium coil. Upon increasing the flow strength $Wi_0$ above $Wi_{0,crit}^{LAOE}(De)$, the conformational space in LAOE adopts a symmetric orthogonal cross shape. This behavior is rationalized by considering that both the $x$- and $y$-axis serve as alternating principal axes of extension in LAOE. As an example, the conformational space for $Wi_0 = 6.5$ and $De = 0.45$ appears as a bright cross, which is consistent with the flow strength above the critical $Wi_{0,crit}^{LAOE}(De) \approx 6.1$ under these conditions. Upon increasing the $Wi_0$ or decreasing the $De$, the shape of the cross sharpens and thins, which is apparent for the case of $Wi_0 = 4.3$ and $De = 0.1$ wherein $Wi_{0,crit}^{LAOE}(De) \approx 1.8 \ll Wi_0 = 4.3$. In general, these observations are consistent with the linear−nonlinear transition behavior in oscillatory extension discussed above.

In addition to the average conformational space, we also investigated the dynamic chain conformations during transitions between stretched states. In prior work, several studies have focused on flow-driven buckling instabilities for semiflexible filaments with $l_p \approx L$ such as actin filaments.[61] However, for globally flexible polymers with $l_p \ll L$, buckling instabilities have also been observed and characterized using optical birefringence.[62] In our work, $\lambda$-DNA molecules have ~400 persistence lengths,[63] which is considered as globally


DOI: 10.1021/acs.macromol.6b01606
Macromolecules 2016, 49, 8018−8030

flexible. We hypothesized that the transient switching of extensional and compressional axes in LAOE could induce buckling in single polymers as bourne out by the appearance of different modes. Figure 8b shows four panels containing a series of single molecule snapshots showing intermediate transition structures during buckling events. For each event, we qualitatively assign the number of modes associated with the buckling event, up to 3-fold events. Figure 8c shows the probability of encountering different buckling events as functions of $Wi_0$ and $De$. The upper panel in Figure 8c shows trends for this behavior upon increasing the flow strength at a constant frequency $De = 0.45$. Upon approaching the critical $Wi_{0,crit}^{LAOE}(De) \approx 6.1$, the occurrence of 1-fold and 2-fold structures increases with flow strength while the occurrence of 3-fold structures decreases. We conjecture that this behavior arises because at higher flow strengths, the role of thermal fluctuations in inducing higher-order modal structures likely lessens. Additionally, we find that DNA stretching at higher $Wi_0$ is facilitated by adopting a lower mode transition structure without returning back to a highly coiled state in LAOE, which experimentally confirms prior predictions that oscillatory extensional flow can enhance the unraveling of DNA molecules by Larson and co-workers.[64] Finally, we also consider the conformational stretching behavior at constant $Wi_0$ (above $Wi_{0,crit}^{LAOE}(De)$) while changing the probing frequency $De$ (lower panel, Figure 8c). At a lower frequency $De = 0.1$ relative to $De = 0.45$, the probability of the coiled structure in the transition increases, which is consistent with the notion that a polymer may have sufficient time to relax to a more compact coiled conformation at low $De$.

## CONCLUSIONS

In this work, we investigate the dynamics of single DNA molecules in small and large amplitude oscillatory extension using a combination of experiments and BD simulations. Good agreement is found between the experimental and simulation results for polymer extension in the $x-y$ plane $l$, the $x$- and $y$-direction projected extensions $l_x$ and $l_y$, and the polymer orientation angle $\phi$. In general, single polymers undergo continuous cycles of compression, rotation, and extension along the $x$- and $y$-axes that can be described by a characteristic periodic cycle. PSDs of polymer extension $l$ and orientation angle $\phi$ show characteristic peaks at $2fT$ and $fT$, respectively, which correspond to periodic extension and reorientation in the oscillatory flow. Moreover, cross-correlation analysis of $x$- and $y$-direction projected extension reveal that $l_x$ and $l_y$ are anticorrelated such that prior negative fluctuations in $l_x$ correspond to positive fluctuations in $l_y$. These results are consistent with the periodic nature of the flow.

We further characterized the average extension of single polymers in oscillatory extensional flow at long times using both experiments and simulations. BD simulations are used to predict the polymer dynamic behavior over a wide range of $Wi_0$ and $De$. Interestingly, average polymer extension in LAOE are self-similar and collapse onto a master average extension curve by defining an effective Weissenberg number $Wi_{eff}$. Physical arguments are used to show that the accumulated fluid strain in a half-cycle is related to the effective Weissenberg $Wi_{eff}$ such that larger amounts of strain result in higher effective flow strengths. Moreover, the definition of $Wi_{eff}$ is further substantiated using analytical model based on a Hookean dumbbell in oscillatory extension. The dynamic behavior of polymers in oscillatory extensional flow is also viewed in the context of two-dimensional Pipkin space defined by $Wi_0$ and $De$, where polymer behavior can be classified into several different regimes as linear or nonlinear or quasi-steady or unsteady. In the present work, we mainly studied dynamics near the boundaries of the linear to nonlinear transitions in LAOE, as shown schematically in Figure 7. Recent work has elucidated the microstructural and stress dynamics for colloids and polymers in LAOS under strongly nonlinear conditions.[65,66] In future work, it would be interesting and informative to study single polymer dynamics in the highly nonlinear, unsteady regime (Regime VI in Figure 7) in the context of high flow strength $Wi_0$ and probing frequency $De$ in LAOE. Finally, the average conformational space and buckling transition structures of single DNA molecules are characterized in LAOE, with probability distributions showing that DNA molecules tend to buckle into lower fold structures at higher flow strengths. Taken together, these results shed new light onto our understanding of nonequilibrium polymer dynamics in time-dependent flows.

## AUTHOR INFORMATION

### Corresponding Author

*E-mail: cms@illinois.edu (C.M.S.).

### Notes

The authors declare no competing financial interest.

## ACKNOWLEDGMENTS

We thank Professor Gareth H. McKinley and Professor Randy H. Ewoldt for helpful discussions and Dr. Kejia Chen for development of image analysis codes. This work was supported by a National Science Foundation (NSF) CAREER Award (CBET-1254340) to C.M.S.

## REFERENCES

(1) Nam, J. G.; Hyun, K.; Ahn, K. H.; Lee, S. J. Prediction of normal stresses under large amplitude oscillatory shear flow. *J. Non-Newtonian Fluid Mech.* **2008**, *150*, 1−10.

(2) Chopra, D.; Vlassopoulos, D.; Hatzikiriakos, S. G. Nonlinear rheological response of phase separating polymer blends: Poly(styrene-co-maleic anhydride)/poly(methyl methacrylate). *J. Rheol.* **2000**, *44*, 27−45.

(3) Debbaut, B.; Burhin, H. Large amplitude oscillatory shear and Fourier-transform rheology for a high-density polyethylene: Experiments and numerical simulation. *J. Rheol.* **2002**, *46*, 1155.

(4) Hyun, K.; Nam, J. G.; Wilhellm, M.; Ahn, K. H.; Lee, S. J. Large amplitude oscillatory shear behavior of PEO-PPO-PEO triblock copolymer solutions. *Rheol. Acta* **2006**, *45*, 239−249.

(5) Klein, C. O.; Spiess, H. W.; Calin, A.; Balan, C.; Wilhelm, M. Separation of the nonlinear oscillatory response into a superposition of linear, strain hardening, strain softening, and wall slip response. *Macromolecules* **2007**, *40*, 4250−4259.

(6) Ferry, J. D. *Viscoelastic Properties of Polymers*, 3rd ed.; John Wiley & Sons: New York, 1980.

(7) Bird, R. B., Armstrong, R. C., Hassager, O., Eds.; *Dynamics of Polymeric Liquids*, 2nd ed.; John Wiley & Sons: New York, 1987; Vol. *1*.

(8) Dealy, J. M.; Wissbrun, K. F. *Melt Rheology and Its Role in Plastics Processing*; Kluwer Academic Publishers: Dordrecht, Netherlands, 1999.

(9) Hyun, K.; Wilhelm, M.; Klein, C. O.; Cho, K. S.; Nam, J. G.; Ahn, K. H.; Lee, S. J.; Ewoldt, R. H.; McKinley, G. H. A review of nonlinear oscillatory shear tests: Analysis and application of large amplitude oscillatory shear (LAOS). *Prog. Polym. Sci.* **2011**, *36*, 1697−1753.

(10) Min Kim, J.; Eberle, A. P. R.; Kate Gurnon, A.; Porcar, L.; Wagner, N. J. The microstructure and rheology of a model, thixotropic



DOI: 10.1021/acs.macromol.6b01606
*Macromolecules* 2016, 49, 8018−8030

nanoparticle gel under steady shear and large amplitude oscillatory shear (LAOS). *J. Rheol.* **2014**, *58*, 1301−1328.
(11) Giacomin, A. J.; Dealy, J. M. In *Techniques in Rheological Measurement*; Collyer, A. A., Ed.; Springer Netherlands:: Dordrecht, 1993; pp 99−120.
(12) Wilhelm, M. Fourier-transform rheology. *Macromol. Mater. Eng.* **2002**, *287*, 83−105.
(13) Yosick, J.; Giacomin, A. J.; Moldenaers, P. A kinetic network model for nonlinear flow behaviour of plastics both in shear and extensional rheology. *J. Non-Newtonian Fluid Mech.* **1997**, *70*, 103−123.
(14) Wilhelm, M.; Maring, D.; Spiess, H.-W. Fourier-transform rheology. *Rheol. Acta* **1998**, *37*, 399−405.
(15) Ewoldt, R. H.; Hosoi, a. E.; McKinley, G. H. New measures for characterizing nonlinear viscoelasticity in large amplitude oscillatory shear. *J. Rheol.* **2008**, *52*, 1427.
(16) Cho, K. S.; Hyun, K.; Ahn, K. H.; Lee, S. J. A geometrical interpretation of large amplitude oscillatory shear response. *J. Rheol.* **2005**, *49*, 747.
(17) Hyun, K.; Kim, S. H.; Ahn, K. H.; Lee, S. J. Large amplitude oscillatory shear as a way to classify the complex fluids. *J. Non-Newtonian Fluid Mech.* **2002**, *107*, 51−65.
(18) Rogers, S. A.; Erwin, B. M.; Vlassopoulos, D.; Cloitre, M. A sequence of physical processes determined and quantified in LAOS: Application to a yield stress fluid. *J. Rheol.* **2011**, *55*, 435.
(19) Radhakrishnan, R.; Underhill, P. T. Oscillatory shear rheology of dilute solutions of flexible polymers interacting with oppositely charged particles. *AIChE J.* **2014**, *60*, 1365−1371.
(20) Mckinley, G. H.; Sridhar, T. Filament-Stretching Rheometry of Complex Fluids. *Annu. Rev. Fluid Mech.* **2002**, *34*, 375−415.
(21) Rasmussen, H. K.; Laillé, P.; Yu, K. Large amplitude oscillatory elongation flow. *Rheol. Acta* **2008**, *47*, 97−103.
(22) Bejenariu, A. G.; Rasmussen, H. K.; Skov, A. L.; Hassager, O.; Frankaer, S. M. Large amplitude oscillatory extension of soft polymeric networks. *Rheol. Acta* **2010**, *49*, 807−814.
(23) Tirtaatmadja, V.; Sridhar, T. A filament stretching device for measurement of extensional viscosity. *J. Rheol.* **1993**, *37*, 1081.
(24) Odell, J. A.; Carrington, S. P. Extensional flow oscillatory rheometry. *J. Non-Newtonian Fluid Mech.* **2006**, *137*, 110−120.
(25) Haward, S. J.; Odell, J. A.; Li, Z.; Yuan, X. F. Extensional rheology of dilute polymer solutions in oscillatory cross-slot flow: The transient behaviour of birefringent strands. *Rheol. Acta* **2010**, *49*, 633−645.
(26) Haward, S. J.; Sharma, V.; Odell, J. A. Extensional opto-rheometry with biofluids and ultra-dilute polymer solutions. *Soft Matter* **2011**, *7*, 9908.
(27) Haward, S. J.; Oliveira, M. S. N.; Alves, M. A.; McKinley, G. H. Optimized cross-slot flow geometry for microfluidic extensional rheometry. *Phys. Rev. Lett.* **2012**, *109*, 1−5.
(28) Perkins, T.; Smith, D.; Larson, R.; Chu, S. Streching of a Single Tethered Polymer in a Uniform Flow. *Science (Washington, DC, U. S.)* **1995**, *268*, 83−87.
(29) Hur, J. S.; Shaqfeh, E. S. G.; Babcock, H. P.; Smith, D. E.; Chu, S. Dynamics of dilute and semidilute DNA solutions in the start-up of shear flow. *J. Rheol.* **2001**, *45*, 421−450.
(30) Smith, D. E.; Babcock, H. P.; Chu, S. Single-polymer dynamics in steady shear flow. *Science (Washington, DC, U. S.)* **1999**, *283*, 1724−1727.
(31) Schroeder, C. M.; Teixeira, R. E.; Shaqfeh, E. S. G.; Chu, S. Dynamics of DNA in the flow-gradient plane of steady shear flow: Observations and simulations. *Macromolecules* **2005**, *38*, 1967−1978.
(32) Schroeder, C. M.; Teixeira, R. E.; Shaqfeh, E. S. G.; Chu, S. Characteristic periodic motion of polymers in shear flow. *Phys. Rev. Lett.* **2005**, *95*, 1−4.
(33) Teixeira, R. E.; Babcock, H. P.; Shaqfeh, E. S. G.; Chu, S. Shear thinning and tumbling dynamics of single polymers in the flow-gradient plane. *Macromolecules* **2005**, *38*, 581−592.
(34) Perkins, T. T.; Smith, D. E.; Chu, S. Single polymer dynamics in an elongational flow. *Science (Washington, DC, U. S.)* **1997**, *276*, 2016−2021.
(35) Smith, D. E.; Chu, S. Response of Flexible Polymers to a Sudden Elongational Flow. *Science (Washington, DC, U. S.)* **1998**, *281*, 1335−1340.
(36) Schroeder, C. M.; Babcock, H. P.; Shaqfeh, E. S. G.; Chu, S. Observation of polymer conformation hysteresis in extensional flow. *Science (Washington, DC, U. S.)* **2003**, *301*, 1515−1519.
(37) Hur, J. S.; Shaqfeh, E. S. G.; Babcock, H. P.; Chu, S. Dynamics and configurational fluctuations of single DNA molecules in linear mixed flows. *Phys. Rev. E: Stat. Phys., Plasmas, Fluids, Relat. Interdiscip. Top.* **2002**, *66*, 3−6.
(38) Babcock, H. P.; Teixeira, R. E.; Hur, J. S.; Shaqfeh, E. S. G.; Chu, S. Visualization of molecular fluctuations near the critical point of the coil-stretch transition in polymer elongation. *Macromolecules* **2003**, *36*, 4544−4548.
(39) Nollert, M. U.; Olbricht, W. L. Macromolecular deformation in periodic extensional flows. *Rheol. Acta* **1985**, *24*, 3−14.
(40) Zhou, Y.; Schroeder, C. M. Single polymer dynamics under large amplitude oscillatory extension. *Phys. Rev. Fluids* **2016**, *1*, 053301.
(41) Kundukad, B.; Yan, J.; Doyle, P. S. Effect of YOYO-1 on the mechanical properties of DNA. *Soft Matter* **2014**, *10*, 9721−9728.
(42) Groisman, A.; Enzelberger, M.; Quake, S. R. Microfluidic memory and control devices. *Science (Washington, DC, U. S.)* **2003**, *300*, 955−958.
(43) Tanyeri, M.; Schroeder, C. M. Manipulation and Confinement of Single Particles Using Fluid Flow. *Nano Lett.* **2013**, *13*, 2357−2364.
(44) Sbalzarini, I. F.; Koumoutsakos, P. Feature point tracking and trajectory analysis for video imaging in cell biology. *J. Struct. Biol.* **2005**, *151*, 182−95.
(45) Schneider, C. A.; Rasband, W. S.; Eliceiri, K. W. NIH Image to ImageJ: 25 years of image analysis. *Nat. Methods* **2012**, *9*, 671−675.
(46) Shenoy, A.; Rao, C. V.; Schroeder, C. M. Stokes trap for multiplexed particle manipulation and assembly using fluidics. *Proc. Natl. Acad. Sci. U. S. A.* **2016**, *113*, 3976−3981.
(47) Perkins, T. T.; Quake, S. R.; Smith, D. E.; Chu, S. Relaxation of a single DNA molecule observed by optical microscopy. *Science (Washington, DC, U. S.)* **1994**, *264*, 822−826.
(48) Chen, K.; Anthony, S. M.; Granick, S. Extending particle tracking capability with delaunay triangulation. *Langmuir* **2014**, *30*, 4760−4766.
(49) Schroeder, C. M.; Shaqfeh, E. S. G.; Chu, S. Effect of Hydrodynamic Interactions on DNA Dynamics in Extensional Flow: Simulation and Single Molecule Experiment. *Macromolecules* **2004**, *37*, 9242−9256.
(50) Öttinger, H. C. *Stochastic Processes in Polymeric Fluids*; Springer-Verlag: Berlin, Germany, 1996.
(51) Doyle, P. S.; Shaqfeh, E. S. G. Dynamic simulation of freely-draining, flexible bead-rod chains: Start-up of extensional and shear flow. *J. Non-Newtonian Fluid Mech.* **1998**, *76*, 43−78.
(52) Somasi, M.; Khomami, B.; Woo, N. J.; Hur, J. S.; Shaqfeh, E. S. G. Brownian dynamics simulations of bead-rod and bead-spring chains: Numerical algorithms and coarse-graining issues. *J. Non-Newtonian Fluid Mech.* **2002**, *108*, 227−255.
(53) Marko, J. F.; Siggia, E. D. Stretching DNA. *Macromolecules* **1995**, *28*, 8759−8770.
(54) Hur, J. S.; Shaqfeh, E. S. G.; Larson, R. G. Brownian dynamics simulations of single DNA molecules in shear flow. *J. Rheol.* **2000**, *44*, 713.
(55) Jendrejack, R. M.; de Pablo, J. J.; Graham, M. D.; Jendrejack, R. M.; Pablo, J. J. D.; Graham, M. D. Stochastic simulations of DNA in flow: Dynamics and the effects of hydrodynamic interactions. *J. Chem. Phys.* **2002**, *116*, 7752−7759.
(56) Press, W. H.; Teukolsky, S. A.; Vetterling, W. T.; Flannery, B. P. *Numerical Recipes: The Art of Scientific Computing*, 3rd ed.; Cambridge University Press: New York, 2007.


DOI: 10.1021/acs.macromol.6b01606
*Macromolecules* 2016, 49, 8018−8030

(57) Bird, R. B., Armstrong, R. C., Hassager, O., Eds.; *Dynamics of Polymeric Liquids*, 2nd ed.; John Wiley & Sons: New York, 1987; Vol. 2.
(58) Pipkin, A. C. *Lectures on Viscoelasticity Theory*; Springer-Verlag: New York, 1972.
(59) Larson, R. G.; Magda, J. J. Coil-stretch transitions in mixed shear and extensional flows of dilute polymer solutions. *Macromolecules* **1989**, *22*, 3004−3010.
(60) Zhou, L.; Cook, L. P.; McKinley, G. H. Probing shear-banding transitions of the VCM model for entangled wormlike micellar solutions using large amplitude oscillatory shear (LAOS) deformations. *J. Non-Newtonian Fluid Mech.* **2010**, *165*, 1462−1472.
(61) Kantsler, V.; Goldstein, R. E. Fluctuations, dynamics, and the stretch-coil transition of single actin filaments in extensional flows. *Phys. Rev. Lett.* **2012**, *108*, 1−5.
(62) Haward, S. J. Buckling instabilities in dilute polymer solution elastic strands. *Rheol. Acta* **2010**, *49*, 1219−1225.
(63) Bustamante, C.; Marko, J.; Siggia, E.; Smith, S. Entropic Elasticity of lambda-Phage DNA. *Science* **1994**, *265*, 1599−1600.
(64) Larson, R. G. The role of molecular folds and 'pre-conditioning' in the unraveling of polymer molecules during extensional flow. *J. Non-Newtonian Fluid Mech.* **2000**, *94*, 37−45.
(65) Khair, A. S. On a suspension of nearly spherical colloidal particles under large-amplitude oscillatory shear flow. *J. Fluid Mech.* **2016**, *791*, R5.
(66) Khair, A. S. Large amplitude oscillatory shear of the Giesekus model. *J. Rheol.* **2016**, *60*, 257−266.



DOI: 10.1021/acs.macromol.6b01606
*Macromolecules* 2016, 49, 8018−8030